IOP Publishing Superconductor Science and Technology
Supercond. Sci. Technol. 31 (2018) 055015 (5pp) https://doi.org/10.1088/1361-6668/aaba67

Inductance analysis of superconducting quantum interference devices with 3D nano-bridge junctions

Hao Wang[1,2], Ruoting Yang[1,2], Guanqun Li[1,2], Long Wu[1,2], Xiaoyu Liu[1], Lei Chen[1,4], Jie Ren[1,4] and Zhen Wang[1,2,3,4]

[1] CAS Center for Excellence in Superconducting Electronics (CENSE), State Key Laboratory of Functional Material for Informatics, Shanghai Institute of Microsystem and Information Technology (SIMIT), Chinese Academy of Sciences (CAS), Shanghai 200050, People's Republic of China
[2] University of Chinese Academy of Science, Beijing 100049, People's Republic of China
[3] School of Physical Science and Technology, Shanghai Tech University, Shanghai 200031, People's Republic of China

E-mail: leichen@mail.sim.ac.cn, jieren@mail.sim.ac.cn and zwang@mail.sim.ac.cn

Received 9 February 2018, revised 26 March 2018
Accepted for publication 28 March 2018
Published 13 April 2018

Abstract

Superconducting quantum interference devices (SQUIDs) with 3D nano-bridge junctions can be miniaturized into nano-SQUIDs that are able to sense a few spins in a large magnetic field. Among all device parameters, the inductance is key to the performance of SQUIDs with 3D nano-bridge junctions. Here, we measured the critical-current magnetic flux modulation curves of 12 devices with three design types using a current strip-line directly coupled to the SQUID loop. A best flux modulation depth of 71% was achieved for our 3D Nb SQUID. From the modulation curves, we extracted the inductance values of the current stripe-line in each design and compared them with the corresponding simulation results of InductEX. In this way, London penetration depths of 110 and 420 nm were determined for our Nb (niobium) and NbN (niobium nitride) films, respectively. Furthermore, we showed that inductances of 11 and 119 pH for Nb and NbN 3D nano-bridge junctions, respectively, dominated the total inductance of our SQUID loops which are 23 pH for Nb and 255 pH for NbN. A screening parameter being equal to one suggests optimal critical currents of 89.6 and 8.1 μA for Nb and NbN SQUIDs, respectively. Additionally, intrinsic flux noise of 110 $\pm$ 40 $n\Phi_0/(\mathrm{Hz})^{1/2}$ is calculated for the Nb SQUIDs with 3D nano-bridge junctions by Langevin simulation.

Keywords: inductance, nano-SQUID, 3D nano-bridge junction, London penetration depth, screening parameter

(Some figures may appear in colour only in the online journal)

Nano-scale superconducting quantum interference devices (Nano-SQUIDs) are supersensitive microscopic magnetic sensors, used for the studies of solid-state qubits, high-resolution scanning SQUID microscopy, inductive transition edge sensors, and magnetic characterization of small samples [1–3]. Nano-SQUIDs of constriction junctions are easily fabricated but suffer from poor modulation depth. A 3D nano-bridge junction was developed, which not only improved the current-phase relation, but also decreased the inductance of the device [4–6]. Compared with tunneling junctions, the capacitance of the junction was negligible, and the inductance become an important constant [7]. It has been proposed to use the kinetic inductance of the nano-bridge junction to store the flux quanta of the SFQ circuit [8]. Also, it has been demonstrated that a nano-bridge junction can be used to operate nano-SQUIDs as a magnetic flux bias [9]. Additionally, the coupling between the SQUID and external samples also correlated with the inductance of the SQUID loop [10–13]. A superconducting

[4] Authors to whom any correspondence should be addressed.

constriction embedded into the SQUID loop has been suggested to increase the coupling to external spins. However, direct measurements of the inductance of nano-SQUIDs are difficult. Many groups have estimated the inductance values of their SQUIDs [9, 14–16]. Owing to differences in the materials, structures and growth processes of superconducting film, these values show a wide variation.

Many simulation tools can now be used to calculate the inductance of a superconducting structure by the finite element method analysis [17–22]. However, the actual London penetration depth is required for accurate simulations. Here, we resorted to a current strip-line directly coupled to the SQUID loop and measured the critical-current magnetic flux modulation curves of 12 devices with three types of design. The best Nb device achieved a flux modulation depth of 71%. Therefore, the inductance values of the current stripe-line could be extracted and compared with the corresponding simulation results of InductEX to determine the London penetration depth of our Nb and NbN films. Optimal critical currents of 89.6 and 8.1 μA are suggested for our Nb and NbN SQUIDs, respectively, satisfying the condition of the screen parameter being equal to one. The intrinsic flux noise of 110 $\pm$ 40 $n\Phi_0/(\mathrm{Hz})^{1/2}$ were estimated for the Nb SQUIDs.

Our SQUIDs with 3D nano-bridge junctions were fabricated using the process reported in [6, 23]. This process is compatible with superconducting materials, including Nb (niobium) and NbN (niobium nitride). The shape of the SQUIDs was designed in a manner containing a flux bias stripe-line across the SQUID loop, as shown in figure 1. According to the geometric dimension and superconducting material, the designed SQUIDs were defined as Shape A-Nb, Shape A-NbN, and Shape B-Nb, as shown in figures 1(a)–(c), respectively. Shape A was defined by Stepper photolithography with a thinner line-width, while Shape B was defined by contact-mode photolithography. In addition, the nano-bridge junctions of Shape A was made by reactive ion etching out of a thin Nb or NbN film, while the ones of Shape B was patterned on resist first and formed by lift-off. The dimension of each design is listed in table 1.

The current I_{stripe} flowing through the stripe-line, generated magnetic flux, which was captured by the superconducting loop of the SQUIDs. The amount of magnetic flux captured could be written as $\Phi = M_{\mathrm{mod\text{-}exp}} \times I_{\mathrm{stripe}}$ [14], where $M_{\mathrm{mod\text{-}exp}}$ is the mutual inductance between the dash-line rectangle and SQUID, as shown in figure 1. Because $M_{\mathrm{mod\text{-}exp}}$ is very close to the inductance of the dash-line rectangle $L_{\mathrm{mod\text{-}exp}}$, we can also write $L_{\mathrm{mod\text{-}exp}} \approx \Phi/I_{\mathrm{stripe}}$ [24]. The size of the rectangle is defined by the width W, height H, and thickness T with $W = 3\ \mu$m, $H = 600$ nm, $T = 150$ nm for Shape A with Nb, $W = 3\ \mu$m, $H = 600$ nm, $T = 100$ nm for Shape A with NbN and $W = 9\ \mu$m, $H = 5.5\ \mu$m, $T = 130$ nm for Shape B, respectively. An equivalent electrical circuit of SQUID is shown in figure 1(d). By sweeping I_{stripe}, the flux modulation curves of the SQUIDs could be measured, as is shown in figure 2. In figure 2, the critical current I_c was normalized to the critical current at the constructive interference $I_{c\text{-max}}$ of each device for comparison, and $I_{c\text{-max}}$ of each device is listed in table 2. We measured the

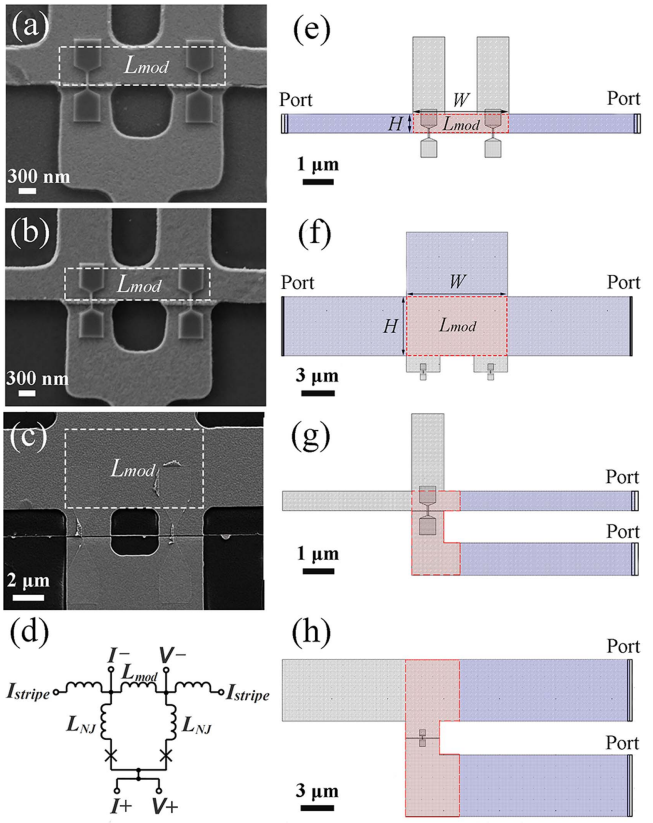

Figure 1. (a)–(c) Top view scanning electron microscopy (SEM) images of SQUIDs with 3D nano-bridge junctions of Shape A-Nb, Shape A-NbN, and Shape B-Nb, respectively. (d) Equivalent electrical circuit of SQUIDs. (e) and (f) Simulation layouts of superconducting structures to calculated inductances of stripe-lines. (g) and (h) Simulation layouts of superconducting structures to calculate inductances of half SQUID loops.

flux modulation curves of the 12 devices of three designs, namely Shape A-Nb, Shape A-NbN, and Shape B-Nb. Each four devices for the same design were fabricated on a single substrate during a same run of fabrication. The variation of $I_{c\text{-max}}$ for the same design and the same superconducting material was likely caused by the uncontrollable roughness of the insulating slits under the nano-bridge junctions [6]. Despite the variation of $I_{c\text{-max}}$, the current I_{period} of I_{stripe} to generate a flux quanta was the same for each kind, as is shown in table 2. The devices of Shape A-Nb, Shape A-NbN, and Shape B-Nb had a I_{period} of 2.4 $\pm$ 0.15, 0.2 $\pm$ 0.01, and 1.77 $\pm$ 0.04 mA, respectively. The $L_{\mathrm{mod\text{-}exp}}$ can be induced as $L_{\mathrm{mod\text{-}exp}} = \Phi_0/I_{\mathrm{period}}$. Therefore, the experimentally measured inductances of the devices Shape A-Nb, Shape A-NbN, and Shape B-Nb were 0.85 $\pm$ 0.05, 10.2 $\pm$ 0.3, 1.17 $\pm$ 0.03 pH, respectively, as shown in table 1.

Because we have the exact geometric dimensions (width W, height H, and film thickness T) of the dashed rectangle, as shown in figure 1, we can numerically simulate the inductance of L_{mod} by electromagnetic finite element analysis. Here, we used a software called InductEx, which was developed to enable circuit designers to extract the inductance of superconducting integrated circuits [17–20]. The software uses numerical engines to calculate the current distribution

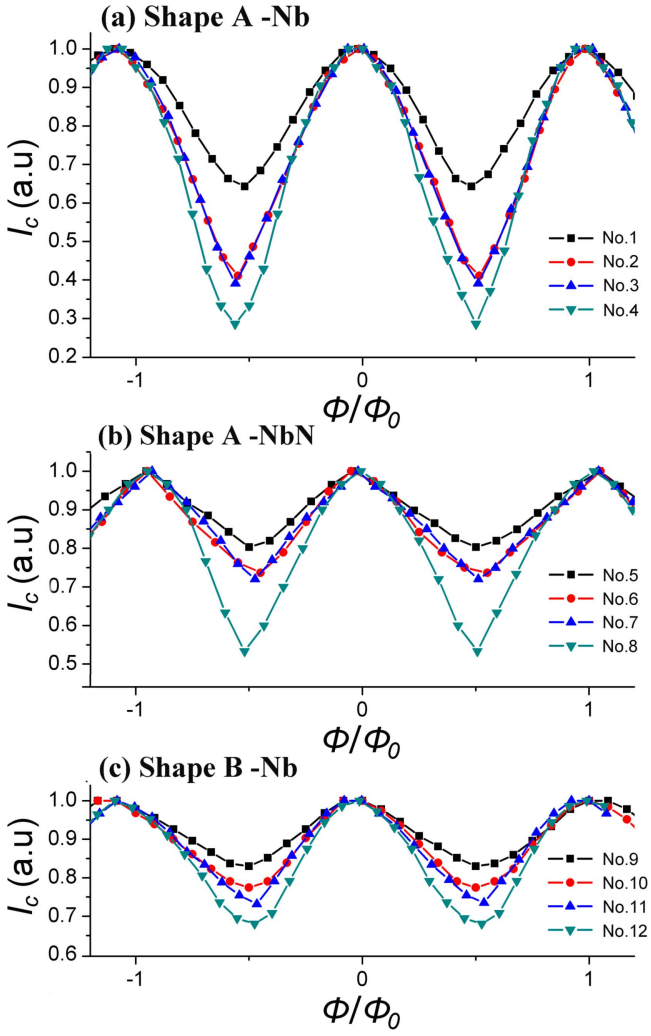

Figure 2. (a)–(c) Critical-current magnetic flux modulation curves of SQUIDs in design Shape A-Nb, Shape A-NbN, and Shape B-Nb, respectively. The critical current was normalized for comparison and the respective normalization factors $I_{c\text{-max}}$ are listed in table.

over the superconducting structure and the corresponding inductance. It reads the layout file of superconducting structures profiled by the red dash line (gray shadows), as shown in figures 1(e) and (f). Because the same shape and size of Shape A-Nb and Shape A-NbN, the layout was shown in one figure of figure 1(d). In the layout file, the current flow in and out port were extended by a 4 and 11 μm along the superconducting line that is profiled by blue dotted lines (blue shadows) for shape A and B, respectively. We then obtained the inductance of the red dashed structure by subtracting the inductance of the blue dotted part of the whole structure. In this way, the virtual influence of the port owing to boundary conditions was minimized in the simulation.

One important input parameter for the simulation is the London penetration depth λ of the superconducting film, which is different owing to the superconducting material, the substrate and the growing process. In the literature, the London penetration depths were $\lambda_{\text{Nb}} = 90$ nm for the Nb film [25] and $\lambda_{\text{NbN}} = 380$ nm for the NbN film [26] on SiO_2 substrates. On the basis of values from the literature, the simulated inductances $L_{\text{mod-sim}}$ of the dashed rectangle in figure 1 were 0.7 ± 0.1, 8.5 ± 0.4, and 1.09 ± 0.03 pH for Shape A-Nb, Shape A-NbN, and Shape B-Nb, respectively, as listed in table 1. The uncertainty of simulated inductances is given by assuming ± 10 nm uncertainty in λ. In comparison, the simulated values were slightly smaller than the corresponding experimentally measured inductance $L_{\text{mod-exp}}$. Therefore, we tuned up the input London penetration depths ($\lambda_{\text{Nb}} = 110 \pm 10$ nm and $\lambda_{\text{NbN}} = 420 \pm 10$ nm) so that $L_{\text{mod-sim}}$ was consistent with the corresponding $L_{\text{mod-exp}}$, as listed in table 1. Here, $\lambda_{\text{NbN}} = 420 \pm 10$ nm also agrees well with a recent literature value of 410 nm for the NbN film [27].

Furthermore, the inductance of the SQUID L_{SQUID} and the nano-bridge junctions L_{NJ} could be simulated in the same way. As shown in figures 1(g) and (h), the structure layout of the half part of the SQUID loop was defined according to the geometric size of the SQUID as the profile of the red dashed line. The current flow in and out of the port could also be extended to exclude the virtual influence of the boundary condition. The L_{SQUID} was twice as large as the simulation result of the half part of the SQUID loop. According to a comparison of the simulated and measured L_{mod} values, the London penetration depth λ for simulation we used here was 110 nm for the Nb film and 420 nm for the NbN film, which was closer to our actual fabrication process. We also simulated the loop inductance L_{loop}, which supposed there was no insulated slit and the two superconducting banks on both sides of the nano-bridge junction were fully connected. We calculated $L_{\text{NJ}} = (L_{\text{SQUID}} - L_{\text{loop}})/2$. In this way we obtained $L_{\text{SQUID}} = 23 \pm 4$, 255 ± 12, and 16 ± 3 pH for devices of Shape A-Nb, Shape A-NbN, and Shape B-Nb, respectively, as it is listed in table 1. L_{NJ} is equal to 11 ± 2 pH, 119 ± 6 pH and 7 ± 1 pH for the shape A-Nb, shape A-NbN and shape B-Nb single nano-bridge junctions, respectively. Here, the width of nano-bridges is 50 nm for shape A and 100 nm for shape B with the thickness of 10 nm.

As shown in figure 2, the flux modulation depth varied with the critical currents of the devices. We defined the flux modulation depth as $\Delta I_c/I_{c\text{-max}} = (I_{c\text{-max}} - I_{c\text{-min}})/I_{c\text{-max}}$, here $I_{c\text{-max}}$ and $I_{c\text{-min}}$ are the critical currents at the constructive and destructive interference of the SQUID, respectively. The value of $\Delta I_c/I_{c\text{-max}}$ as a function of $I_{c\text{-max}}$ was plotted in the inset of figure 3. The $\Delta I_c/I_{c\text{-max}}$ of the Shape A-Nb, Shape A-NbN and Shape B-Nb SQUIDs reached values of 71%, 47% and 32% when $I_{c\text{-max}}$ was 10.5, 15 and 69 μA, respectively. Using the L_{SQUID} simulated above, we calculated the screening parameter $\beta_L = I_{c\text{-max}} L_{\text{SQUID}}/\Phi_0$ of the SQUIDs, and plotted $\Delta I_c/I_{c\text{-max}}$ as a function of β_L, as shown in figure 3. The continuous solid lines are provided as eye-guide lines to show the rough trend of the modulation depth as the function of β_L. When β_L of the SQUID was in the region of $\beta_L < 1$, $\Delta I_c/I_{c\text{-max}}$ saturation occurred at 73%, 55% and 45% for the Shape A-Nb, Shape A-NbN and Shape B-Nb devices. The inductance of a SQUID is mainly dominated by the nano-bridge junctions; hence, tuning down the critical current is a direct way to improve the modulation depth of the SQUID. For the Shape A and Shape B Nb SQUIDs, $I_{c\text{-max}} = 89.6$ and 130.2 μA with $\beta_L = 1$ respectively, is a good value for an Nb

Table 1. The values of the dimension (width × height × thickness), the measured inductance $L_{\text{mod-exp}}$, the simulated inductance $L_{\text{mod-sim}}$ of flux strip-line in the three designs, with London penetration depths λ, inductance of the whole SQUID loop L_{SQUID}, and inductance of the single nano-bridge junction L_{NJ}.

	Shape A-Nb	Shape A-NbN	Shape B-Nb
L_{mod} size ($W \times H \times T$)	3 μm × 0.6 μm × 0.15 μm	3 μm × 0.6 m × 0.1 μm	9 μm × 5.5 μm × 0.13 μm
$L_{\text{mod-exp}}$	0.85 ± 0.05 pH	10.2 ± 0.3 pH	1.17 ± 0.03 pH
$L_{\text{mod-sim}}$ ($\lambda_{\text{Nb}} = 90 \pm 10$ nm, $\lambda_{\text{NbN}} = 380 \pm 10$ nm)	0.67 ± 0.09 pH	8.5 ± 0.4 pH	1.09 ± 0.03 pH
$L_{\text{mod-sim}}$ ($\lambda_{\text{Nb}} = 110 \pm 10$ nm, $\lambda_{\text{NbN}} = 420 \pm 10$ nm)	0.9 ± 0.1 pH	10.2 ± 0.5 pH	1.15 ± 0.04 pH
L_{SQUID} ($\lambda_{\text{Nb}} = 110 \pm 10$ nm, $\lambda_{\text{NbN}} = 420 \pm 10$ nm)	23 ± 4 pH	255 ± 12 pH	16 ± 3 pH
L_{NJ} ($\lambda_{\text{Nb}} = 110 \pm 10$ nm, $\lambda_{\text{NbN}} = 420 \pm 10$ nm)	11 ± 2 pH	119 ± 6 pH	7 ± 1 pH

Table 2. The maximum critical current $I_{c\text{-max}}$, flux modulation depth $\Delta I_c/I_{c\text{-max}}$, and modulation period I_{period} of the devices, and the normal resistance R_n of each SQUID.

	Shape A-Nb				Shape A-NbN				Shape B-Nb			
No.	1	2	3	4	5	6	7	8	9	10	11	12
$I_{c\text{-max}}$ (μA)	196	144	46	10.5	61	38	25	15	216	119	85	69
$\Delta I_c/I_{c\text{-max}}$	0.36	0.58	0.61	0.71	0.2	0.26	0.28	0.47	0.17	0.23	0.27	0.32
I_{period}(mA/Φ_0)	2.44	2.63	2.26	2.4	0.2	0.2	0.2	0.21	1.8	1.8	1.73	1.73
R_n (Ω)	4.2	4.6	11.8	18.7	57.7	68.5	76.4	88.1	9.5	12.1	13.9	16.2

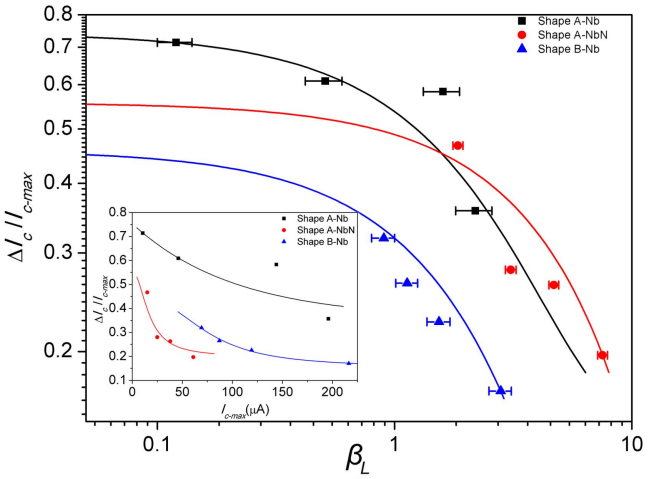

Figure 3 Flux modulation depth $\Delta I_c/I_{c\text{-max}}$ as a function of the screening parameter β_L. Insert shows the $\Delta I_c/I_{c\text{-max}}$ as a function of critical current I_c. $\Delta I_c/I_{c\text{-max}}$ and I_c were calculated from the devices for which the flux modulation curves were plotted in figure 2.

SQUID. However, the inductance of the Shape A-NbN SQUID was much greater and requires the device to have a critical current less than 8.1 μA for $\beta_L < 1$. Furthermore, it is known that SQUIDs with ideal Josephson junctions will reach $\Delta I_c/I_{c\text{-max}} = 100\%$ when $\beta_L < 1$. Although the current-phase relation of the 3D nano-bridge junctions has been improved considerably, $\Delta I_c/I_{c\text{-max}}$ as a function of β_L saturated at 73%, 55% and 45% in figure 3 indicating a non-ideal Josephson junction. The max modulation depth given by the KO-1 model for weak link junctions is 81% [5]. This result indicates that the effective length of the 3D nano-bridge junctions of Shape A-Nb SQUIDs approaches the superconducting coherence length of Nb films, while the nano-bridge junctions of Shape A-NbN and Shape B-Nb is still too long. For NbN SQUIDs, it is expected because of the short coherence length of the NbN film. For Shape B-Nb SQUIDs, the nano-bridge junctions are made of lift-off which is not ideal for a good contact between the nano-bridge junction layer and underneath superconducting banks. Therefore, the effective junction length of Shape B-Nb is longer than one of Shape A-Nb, which is also reflected in the greater normal resistance R_n values of Shape B-Nb SQUIDs for similar $I_{c\text{-max}}$ values. As listed in table 2, the normal resistance R_n of each SQUID obtained from the derivative of voltage with respect to current at the normal state.

Despite an optimal critical current $I_{c\text{-max}}$, it is not easy to control the critical current of 3D nano-bridge junctions, which is indicated by the variation of $I_{c\text{-max}}$ of the devices with the exact same design. There are many factors that determine the critical current of 3D nano-bridge junctions, such as the junction dimension, the material composition of the junctions, and the electric-magnetic noise going through junctions. The variation of R_n indicated that the actual dimensions of the 3D nano-bridge junctions were not the same. We believe that the roughness across the surface of the insulating slit under the nano-bridge left by the lift-off step was responsible for the uncertainty of the actual dimensions (as figures 1(b) and (c) in [6]). Chemical (or mechanical) polishing might be required to remove the roughness before setting the nano-bridges in order to improve the reproducibility of the normal resistance R_n of SQUIDs.

Since 3D nano-bridge junctions of Shape A-Nb SQUIDs are approaching ideal Josephson junctions, their theoretic intrinsic flux noise can roughly estimated by Langevin simulation, $S_\Phi{}^{1/2} = [f(\beta_L)\Phi_0 k_B T L_{\text{SQUID}}/I_{c\text{-max}}R_n]^{1/2}$, when $\beta_c \leqslant 1$ [14, 28], where k_B is the Boltzmann constant, T is the

temperature, and R_n is the normal resistance of junctions. For $\beta_L > 0.4, f(\beta_L) \approx 4(1 + \beta_L)$. The $I_{c\text{-max}}R_n$ values were equal to 0.56 ± 0.27 mV for nano-bridge junctions of Shape A-Nb SQUIDs. We assumed that it is possible to make a SQUID with $\beta_L = 1$ with optimal critical currents. Therefore, the theoretic intrinsic flux noise for Shape A-Nb SQUIDs with 3D nano-bridge junctions are $S_\Phi{}^{1/2} = 110 \pm 40\ n\Phi_0/(\text{Hz})^{1/2}$ at $T = 4.2$ K, which is the temperature of liquid helium. For a non-ideal Josephson current-phase relation, the estimation of the intrinsic noise of Shape A-NbN and Shape B-Nb SQUIDs will require knowing of the exact effective length of the 3D nano-bridge junctions to perform a more detailed simulation [29].

In conclusion, we have measured critical-current magnetic flux modulation curves of twelve SQUIDs with 3D nano-bridge junctions. We have used a current strip-line directly coupled to the SQUID loop to apply the magnetic flux so that we can extract the inductance of that piece of superconducting line. With a comparison to the simulated inductance values by InductEX, London penetration depths of 110 and 420 nm for our Nb and NbN films were determined. Furthermore, we simulated the inductance of Nb and NbN SQUID 3D nano-bridge junctions as 11 and 119 pH, respectively, dominated the total inductance of our SQUID loops which are 23 pH for Nb and 255 pH for NbN. The flux modulation depth $\Delta I_c/I_{c\text{-max}}$ as a function of the screening parameter β_L was plotted. The modulation depths of Nb and NbN SQUID were expected to reach saturation at 73% and 55%, respectively. Therefore, optimal critical currents of 89.6 and 8.1 μA were suggested for Nb and NbN SQUIDs. The intrinsic flux noise of $110 \pm 40\ n\Phi_0/(\text{Hz})^{1/2}$ was estimated for Nb SQUIDs by Langevin simulation.

Acknowledgments

We gratefully acknowledge support from the National Key R&D Program of China (2017YFF0206105), the Frontier Science Key Programs of the Chinese Academy of Sciences (Grant No. QYZDY-SSW-JSC033), the one-hundred-person project of the Chinese Academy of Science, the National Science Foundation of China (Grant No. 61601445), and Shanghai Science and Technology Committee (Grant No. 17JC1401100).

ORCID iDs

Lei Chen https://orcid.org/0000-0002-4746-5441

References

[1] Foley C P and Hilgenkamp H 2009 *Supercond. Sci. Technol.* **22** 064001
[2] Rugar D, Budakian R, Mamin H J and Chui B W 2004 *Nature* **430** 329–32
[3] Denis V *et al* 2013 *Nat. Nanotechnol.* **8** 639–44
[4] Faucher M, Fournier T, Pannetier B, Thirion C, Wernsdorfer W, Villegier J C and Bouchiat V 2002 *Physica* C **368** 211–7
[5] Vijay R, Levenson-Falk E M, Slichter D H and Siddiqi I 2010 *Appl. Phys. Lett.* **96** 223112
[6] Chen L, Wang H, Liu X, Wu L and Wang Z 2016 *Nano Lett.* **16** 7726–30
[7] Granata C and Vettoliere A 2016 *Phys. Rep.* **614** 1–69
[8] Andrew M, Dmitri V A and Alexey B 2017 *New J. Phys.* **19** 063015
[9] McCaughan A N, Zhao Q and Berggren K K 2016 *Sci. Rep.* **6** 28095
[10] Wölbing R, Schwarz T, Müller B, Nagel J, Kemmler M, Kleiner R and Koelle D 2014 *Supercond. Sci. Technol.* **27** 125007
[11] Bouchiat V 2009 *Supercond. Sci. Technol.* **22** 064002
[12] Kirtley J R *et al* 2016 *Supercond. Sci. Technol.* **29** 124001
[13] Kirtley J R *et al* 2016 *Rev. Sci. Instrum.* **87** 093702
[14] Schwarz T, Nagel J, Wölbing R, Kemmler M, Kleiner R and Koelle D 2013 *ACS Nano* **7** 844–50
[15] Russo R *et al* 2017 *Supercond. Sci. Technol.* **30** 024009
[16] Hasselbach K, Mailly D and Kirtley J R 2002 *J. Appl. Phys.* **91** 4432–7
[17] Coenrad J F *et al* 2011 *Supercond. Sci. Technol.* **24** 125015
[18] Coenrad J F *et al* 2013 *IEEE Trans. Appl. Supercond.* **23** 1300705
[19] Coenrad J F *et al* 2013 *Supercond. Sci. Technol.* **26** 015016
[20] Coenrad J F *et al* 2015 *IEEE Trans. Appl. Supercond.* **25** 1300209
[21] Khapaev M M *et al* 2003 *Supercond. Sci. Technol.* **16** 24
[22] Khapaev M M *et al* 2001 *IEEE Trans. Appl. Supercond.* **11** 1090–3
[23] Wang H, Chen L, Liu X, Wu L, Wu X, You L and Wang Z 2017 *IEEE Trans. Appl. Supercond.* **27** 1601905
[24] Ren J *et al* 2009 *IEEE Trans. Appl. Supercond.* **19** 961
[25] Ilin K S, Vitusevich S A, Jin B B, Gubin A I, Klein N and Siegel M 2004 *Physica* C **408–410** 700–2
[26] Lisitskiy M *et al* 2014 *J. Appl. Phys.* **116** 043905
[27] Kubo S, Asahi M, Hikita M and Igarashi M 1984 *Appl. Phys. Lett.* **44** 258–60
[28] Clarke J and Braginski A I 2004 *The SQUID Handbook* vol 1 (Weinheim: Wiley-VCH) ch 2
[29] Granata C *et al* 2011 *Phys. Rev.* B **84** 224516